The friction and wear of Kevlar 49 sliding against aluminium at low velocity under high contact pressures.

I.F. Brown *, C.J. Burgoyne

Engineering Department, University of Cambridge, Trumpington Street, Cambridge, England, CB2 1PZ.

Abstract

The friction and wear behaviour of Kevlar 49 sliding against aluminium under large contact pressures at low sliding velocities was examined. Medium scale tests using yarns of 1000 filaments around capstan discs of radii 10-80mm were performed; these are compared with large scale tests on 6 and 60 tonne rope terminations. In both situations the number of cycles to failure for a given severity regime is recorded. The wear rate is found to be proportional to the normal load for five orders of magnitude of load. The dimensional coefficient of wear in the Archard wear equation is estimated from the given severities, and is found to increase with increasing amplitude of slip.

Kevlar 49 on aluminium friction is measured using yarns on capstans, and compared with literature results for Kevlar 49 on itself. A modified version of Howell's equation is presented in terms of stresses, $\tau = a\sigma^{\beta}$, to allow finite element modelling of rope terminations. For Kevlar 49-on-aluminium this takes the form $\tau_s = 0.099\sigma^{0.91}$ and $\tau_d = 0.095\sigma^{0.91}$. Kevlar 49-on-Kevlar 49 friction is not so critical in the mechanics of the terminations as it is greater ($\mu \rightarrow 0.22$ at high pressures). In a similar way, Kevlar 49-on-Kevlar 49 abrasion is not assumed to be the critical factor in the lifetimes of terminations, Kevlar 49-on-aluminium abrasion is. It is found here that the wear rate is directly proportional to the normal load so Kevlar 49-on-aluminium abrasion can be expressed in terms the Archard wear equation. The dimensional wear coefficient is found to depend stongly on the amplitude of slip present, rising from $1.0 \times 10^{-5}\text{mm}^3(\text{Nm})^{-1}$ at 40μm to $1.0 \times 10^{-2}\text{mm}^3(\text{Nm})^{-1}$ at 3mm peak to peak displacement.

Keywords: Kevlar; Aramid; Friction; Wear; Ropes

1. Introduction

The purpose of these tests was to investigate the mechanics within a Kevlar 49 termination as shown in Fig. 1. Ropes made from parallel aramid yarns have been used for many years due to their light weight, good electrical properties and utilisation of the material's stiffness. The standard termination for these parallel-lay (Parafil) ropes is a "spike-and-barrel" developed by the rope manufacturer. The terminations perform very well under static loading but fail due to abrasion of the rope near the nose of the spike when exposed to cyclic stresses.

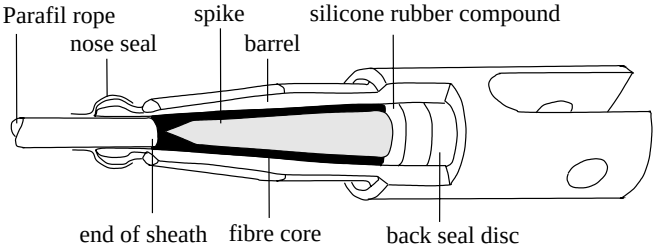

Figure 1: Spike and barrel Parafil termination.

Spike-and-barrel terminations for parallel-lay ropes are much more complex than they first appear. The functioning of the termination is heavily influenced by geometry, the material properties of both the termination and fibre, and the frictional properties. Any alteration to one of these factors alters the behaviour of the whole termination. Over their 25 year history, Parafil terminations have evolved into a sophisticated design which works well most of the time. To improve on their performance this study has looked inside the terminations and exposed hitherto unknown mechanisms and processes of slip and wear [1].

No straightforward analysis is possible because the simplifying assumptions mask the subtleties of the design. The use of a modified Howell's equation for friction, $\tau = a\sigma^{\beta}$, is proposed here as a valid means of modelling the friction between polymeric materials. This re-expression in terms of stress, enables its use in a finite element analysis. Experiments on Kevlar 49 yarns over aluminium capstans were performed to determine the stick and slip coefficients of friction.

Kevlar 49-on-aluminium abrasion tests were performed and the Archard wear equation was applied by devising the contact pressure, amplitude of slip and thickness to be abraded. This equation is also applied to literature data for 6 and 60 tonne Parafil terminations under various cyclic regimes. These two very

*Corresponding author. Hyder Special Structures, 29 Bressenden Place, London, SW1E 5DZ UK. Tel.: +44 171 316 6033; fax: +44 171 316 6215

different scales of tests show a very good agreement.

2. Friction of polymers

When either or both of the surfaces are polymers, the contact is often predominantly elastic. Friction of polymers can be attributed to two sources, deformation and adhesion. The friction due to deformation arises from energy dissipation in the bulk of the polymer as the surfaces slide. The friction due to adhesion arises from the asperities on the two surfaces sticking together, a force is needed to break apart these junctions. In most situations both deformation and adhesion will be present.

Polymers deform viscoelastically: the deformation depends not only on the normal load N but also on the geometry and time of loading.

2.1. Friction due to deformation

Study of this component can be achieved by isolating with metal spheres rolling over lubricated polymer surfaces to reduce interfacial adhesion. Alternatively a slider can be dragged over a well lubricated surface. The friction due to deformation can be calculated by analysing the deformation that occurs within the polymer per unit distance rolled, and calculating the energy that will be dissipated as heat due to the material's viscoelasticity. For the special case of a metal sphere of radius R rolling under a normal load W, the frictional force F_{def} will be given by

$$F_{\text{def}} = 0.17\beta W^{4/3} R^{-2/3} (1-\nu^2)^{1/3} E^{-1/3} \qquad (1)$$

where ν is the Poisson's ratio for the polymer, E is the Young's modulus, and β is the fraction of the total energy dissipated. A good agreement is generally found between eqn. (1) and experimental measurements [2].

2.2. Friction due to adhesion

At low loads and moderately rough surfaces the true area of contact is a small fraction of the apparent area, and is proportional to the normal load. The coefficient of friction is therefore constant and independant of the normal load.

At high loads or for very smooth surfaces, the individual asperities are merged into one large asperity. For a single elastic asperity the area of contact, A, will be proportional to the load, W, raised to the power $2/3$, this exponent applied to both spherical and cylindrical asperities [2]. The shear strength, τ, of polymers varies with the hydrostatic pressure, σ, in the following way:

$$\tau = \tau_0 + \alpha\sigma \qquad (2)$$

where τ_0 and α are constants for the polymer. But $\sigma = W/A$, $F = \tau A$ and $A \propto W^{2/3}$, therefore [3];

$$\mu = bW^{-1/3} + \alpha \qquad (3)$$

where α and b are constants.

For very high pressures (typically greater than 50 MPa [4]) the real contact area is equal to the apparent contact area. Therefore eqn. (2) leads to:

$$\mu = \frac{\tau}{\sigma} = \frac{\tau_0}{\sigma} + \alpha \qquad (4)$$

which tends to the value of α for very high pressures.

2.3. Summation of friction components

Kragelsky et al. [5] support the hypothesis that the coefficient of friction is the sum of two terms; molecular and mechanical, i.e.;

$$\mu = \mu_{molecular} + \mu_{mechanical} \qquad (5)$$

Molecular interaction processes take place in the surface 'film' and affect the surface layers to a depth of a few hundredths of a micron. Mechanical interaction takes place in layers with a thickness of a few tenths of a micron. As these processes occur at different levels they are largely uncorrelated and hence can be separated.

This equation suggests a very complex relationship between the normal load and the coefficient of friction; both components of μ include a pressure term, as well as extra terms for the hysteresis loss during sliding, the surface roughness, and the strength of the molecular bond, amongst others.

2.4. A modified Howell's equation

With fixed geometry and duration of loading, the area of true contact is proportional to N^β where N is the normal load and $\frac{2}{3} \leq \beta \leq 1$. For a truly elastic solid (for example rubber), $\beta = \frac{2}{3}$ [6].

Howell and Mazur [7] performed some of the first experiments to study the effect that the elastic behaviour of the asperity-to-asperity contact has on the nature of sliding for polymeric materials. The stress-strain curves of three hypothetical materials are shown in Fig. 2. The dashed lines represent the stress range in the contacting asperities. The asperities of material (a) deform plastically, so Amontons' law applies. The asperity-to-asperity contact in material (b) is elastic; so the true asperity-on-asperity contact area will be of the form $CN^{2/3}$ where C involves the modulus and dimensions of the asperities, hence $F = SCN^{2/3}$ (where S is the shear breaking strength). Increasing the normal stress would cause plastic deformations as for material (a).

For material (c) the deformation of the asperity contact starts with a linear elastic region followed by a gradual yield; the true asperity-on-asperity contact area is thus likely to lie between the bounds of materials (a) (plastic $A \propto N$) and (b) (elastic $A \propto N^{2/3}$). Therefore a possible equation for the friction could be

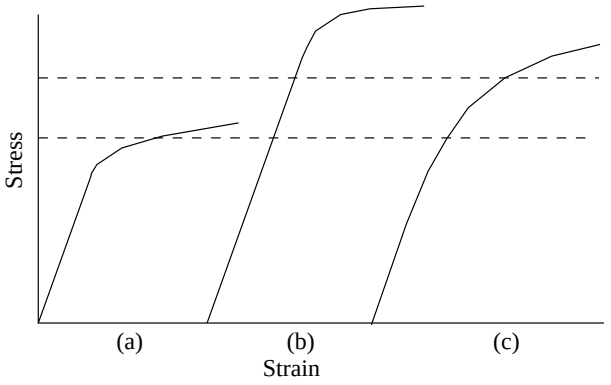

Figure 2: Stress-strain curves for various hypothetical aperity models.

the empirical one, $F = KN^{\beta}$, where $\frac{2}{3} \leq \beta \leq 1$. Most synthetic polymers used in ropes correspond most closely to material (c) where the actual mechanism of asperity deformation is indeterminate.

The relationship $F = KN^{\beta}$ fits Howell and Mazur's test results very well; some of their results are shown in Table 1.

Material	K	β
cellulose acetate	0.60	0.96
viscose rayon	0.49	0.91
drawn nylon	0.92	0.80
undrawn nylon	0.85	0.90

Table 1: Coefficients and indices of friction, $F = KN^{\beta}$, for various polymers. [8]

Howell's equation for friction can be re-written as $F = (KN^{\beta-1})N$, where $(KN^{\beta-1})$ is the "equivalent coefficient of friction". For use in the finite element analysis it was decided that expressing this relationship in terms of stresses would make modelling possible. Therefore, it is proposed here that Howell's equation can be re-expressed by an alternative empirical relationship; $\tau = a\sigma^{\beta}$, where τ is the frictional stress, σ is the contact pressure, and a and β are frictional constants.

Due to the viscoelastic properties of polymers, when a polymer is in contact with another surface for a period of time, the asperities start to creep under the normal load. This increases the actual area of contact, thereby increasing the frictional limit. This creep explains why contact involving polymers typically has a greater difference between static and dynamic coefficients of friction, than for metal-to-metal contact.

2.4..1 Effect of spin finish on friction

Spin finish is a surface coating, added to the fibres during manufacture, for the purpose of gluing together the fibres during the processing of the yarn [9]. This prevents them being snagged by the guides and thus being broken or drawn out of the yarn. The finish also evens out, and so improves, the running properties and friction coefficients, as well as removing any electrostatic charge; these keep the draw-off conditions as even as possible.

Yarn sizes are also used; these coat the yarn with a protective film to reduce the abrasion damage during processing and service.

By selecting the right finish, the abrasion resistance of the yarn can be increased [10, 11, 12, 13]. The yarns used in the tests referred to in this chapter are from spools used to make Parafil ropes and so carry the finishes present in actual rope.

3. Kevlar-on-aluminium friction

3.1. Measurement of yarn-on-capstan friction

The simplest method of measuring the friction between a yarn and a solid is by the capstan method. Here the yarn is pulled over a cylinder of radius R through an angle θ and the end tensions measured (Figs. 3 and 4). Amontons' law leads to (see for example [14]):

$$T_o = T_i \, e^{\mu \theta} \tag{6}$$

which is often referred to as the capstan equation and is independent of R. T_i, the incoming tension, is the tension in the yarn entering the contact zone, between the weights and the capstan. T_o, the outgoing tension, is the tension in the yarn leaving the capstan, between the capstan and the tensometer. μ is the coefficient of friction.

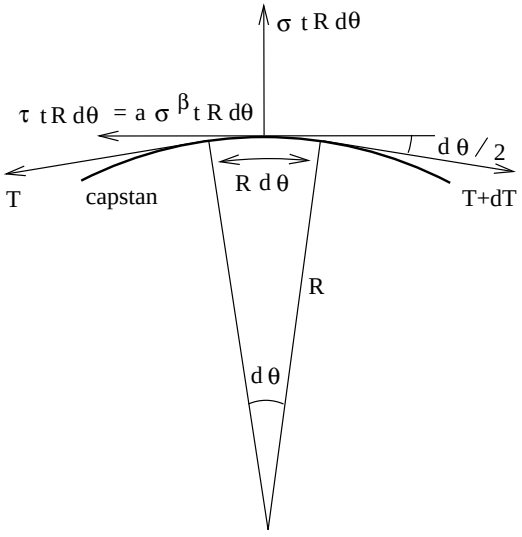

Figure 3: Forces acting on a segment of yarn running over a capstan.

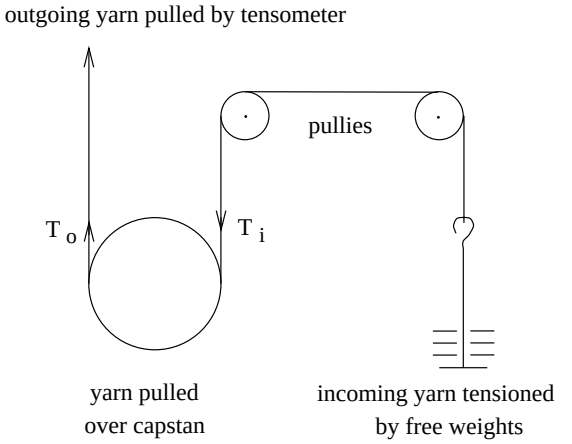

Figure 4: Apparatus used to measure yarn on solid friction.

Howell's [8] equation ($F = KN^{\beta}$) leads to:

$$T_o^{1-\beta} = T_i^{1-\beta} + (1-\beta)\, K\, \theta\, R^{1-\beta} \qquad (7)$$

Thus the radius of the capstan now comes into the equation [16]. If a modified Howell's equation $\tau = a\sigma^{\beta}$ is used then an alternative equation can be derived. (Note: β is a dimensionless index, but a has dimensions of $(\mathrm{FL}^{-2})^{(1-\beta)}$. Therefore care must be taken if the units of σ are changed, as this will change the value of a.)

Consider a small element of yarn subtending an angle $\mathrm{d}\theta$ around a capstan, as shown in Fig. 3. The radius is R, the contact width is t, the contact pressure is σ, and the frictional stress is $\tau = a\sigma^{\beta}$. A resolution of forces along the yarn gives:

$$a\sigma^{\beta} tR\mathrm{d}\theta = \mathrm{d}T \qquad (8)$$

Resolving perpendicular to the contact surface gives:

$$2T\frac{\mathrm{d}\theta}{2} = \sigma tR\mathrm{d}\theta \qquad (9)$$

Eliminating σ from these two equations gives:

$$at^{1-\beta}R^{1-\beta}\mathrm{d}\theta = \frac{1}{T^{\beta}}\mathrm{d}T \qquad (10)$$

This can be integrated between $\theta = 0$ to θ, and $T = T_i$ to T_o, yielding:

$$T_o^{1-\beta} = T_i^{1-\beta} + (1-\beta)\, a\, t^{1-\beta}\, R^{1-\beta}\, \theta \qquad (11)$$

This equation is then fitted to experimental values of T_o and T_i to give the coefficients a and β that are used in the finite element analysis.

The contact width was taken to be 1.0mm, both for this analysis, and for the abrasion analysis in Section 7. This is consistent with observations of the yarns on the various sized capstans.

3.2. Apparatus.

The basic apparatus consists of an aluminium capstan over which a Kevlar yarn is pulled, as shown in Fig. 4. The tension in the yarn leaving the contact zone, (the outgoing tension, T_o), is measured by means of the Howden tensometer to which the yarn is tied. The tension in the yarn entering the contact zone, (the incoming tension, T_i), is derived from the free weights applied plus an allowance for the friction in the two pulleys. This allowance is calculated by pulling loaded yarns over two pulleys with no capstan present. For a given incoming tension the tensometer is moved upwards, stretching the yarn between it and the capstan until the force in the yarn is sufficient to overcome friction and the yarn slips. The use of short lengths of yarn (less than 500mm connecting the tensometer to the capstan), ensures that little energy is stored, so when slipping occurs it is continuous, and not a series of stick-slip jumps.

For the test shown in Fig. 5 the yarn was stopped to allow it to stick, then re-pulled to see if the new force to initiate sliding was the same as the initial one. It could be argued that subsequent forces would differ as the distribution in tension, and hence contact pressure, around the capstan varies slightly between the two. This variation may arise if the incoming tension has not initially worked its way around the capstan, but it can be seen from Fig. 5 that all the static peaks have similar magnitudes.

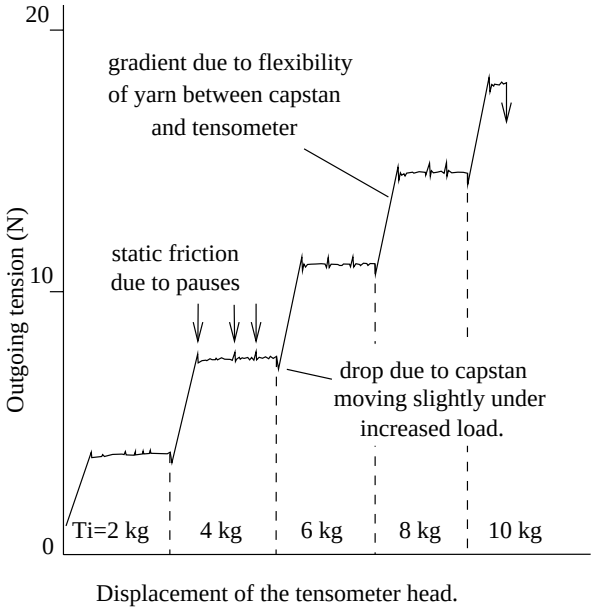

Figure 5: Plot of the outgoing tension for Kevlar 49 pulled over a 30mm aluminium capstan at 0.17mm/s.

It is possible to cycle the tensometer in both directions, such that it measures incoming and outgoing tensions, however this practice excessively reuses one portion of yarn more than the rest. This leads to fairly

rapid abrasion with a fine powder building up on the capstan which affects the measurements taken. So the yarn is pulled in one direction only which results in a continuous intake of clean yarn.

At the start of a test the apparatus is set up with the lowest free weight in place and the tensometer head is raised until slipping takes place. More free weights are added, and the procedure repeated until the yarn snaps, usually at the knot attaching it to the tensometer. Then the test is repeated with a new yarn, ensuring that the earmarked contacting portion is not handled. Between tests the contact area is cleaned with acetone to remove any Kevlar powder that has built up. After many tests it was seen that the aluminium surface had become polished from abrasion. Six tests were each performed on capstans of radii, 10, 20, 30, 40, 50, 60, 70 and 80mm; each test giving between 4 and 6 readings depending on how many loads were applied. 216 readings were taken in total.

3.3. Experimental equivalent coefficient of friction, μ.

Many of the experimental points correspond to low contact stresses, which are not of interest in this analysis. To remove their effect, it is necessary to quantify the contact stresses. A simple analysis for this will suffice, as this is only an indication of the contact stress; eqn. (11) takes into account the variation in contact stress along the length of the contact zone for each and every test.

A mean contact stress, $\overline{\sigma}$, was obtained by assuming a uniform contact pressure around the contacting half of the capstan. Resolving forces on the yarn around the capstan, in a direction parallel to the incoming and outgoing yarns, gives:

$$\overline{\sigma} = (T_o + T_i)/2Rt \tag{12}$$

as shown in Fig. 6. To get a mean frictional stress, $\overline{\tau}$, it was assumed that the frictional stress was constant, so looking at the whole contact area gives:

$$\overline{\tau} = (T_o - T_i)/\pi Rt \tag{13}$$

If one were to assume that Amontons' law applies, then an application of eqn. (6) to the 216 readings of T_o and T_i gives Fig. 7, the contact stress being calculated using eqn. (12). It can be seen that the greater the contact stress the lower the coefficient of friction; this nullifies the assumptions made in deriving this graph, so Amontons' law is not a good model for Kevlar-on-aluminium friction. It is also noted that the coefficient of friction between Kevlar 49 and aluminium is lower than that between Kevlar 49 and itself, which tends to 0.22 at high pressures [3]. This supports the hypothesis that any slip occuring within a Parafil termination does so between the rope and the spike or barrel, rather than within the rope. Therefore the Kevlar 49 on aluminium abrasion will be the dominating factor in the lifetime of a termination.

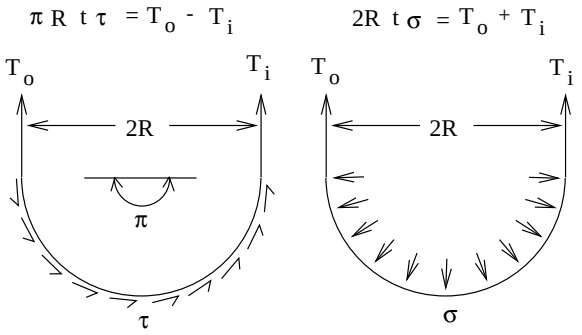

Figure 6: Estimation of average contact and frictional stresses on a capstan.

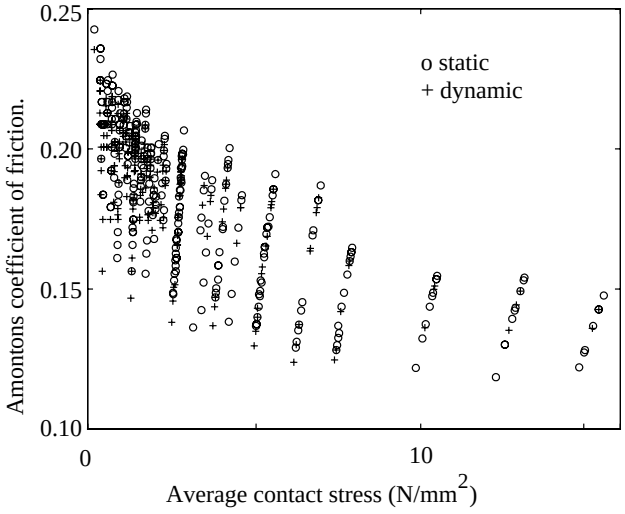

Figure 7: Effective Amontons' coefficient of friction, μ, for Kevlar 49-on-aluminium assuming μ is constant.

Figure 8 shows a plot of $\overline{\tau}$ versus $\overline{\sigma}$. The data points are in pairs; a circle corresponds to a static measurement, and the cross below it corresponds to the accompanying dynamic measurement. It can be seen that the points do not lie on a straight line — at greater contact pressures the effective coefficient of friction reduces.

3.4. Experimental coefficients of friction, a and β.

A best fit equation of the form given in eqn.(11) to all the measured data points (216 static and 216 dynamic) leads to the following two equations:

$$\tau_s = 0.087\sigma^{0.88} \tag{14}$$

$$\tau_d = 0.084\sigma^{0.88} \tag{15}$$

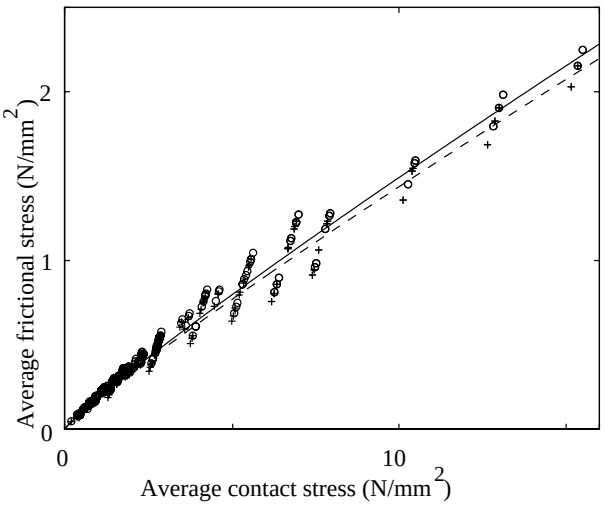

Figure 8: Visualisation of the average frictional stress versus average contact stress.

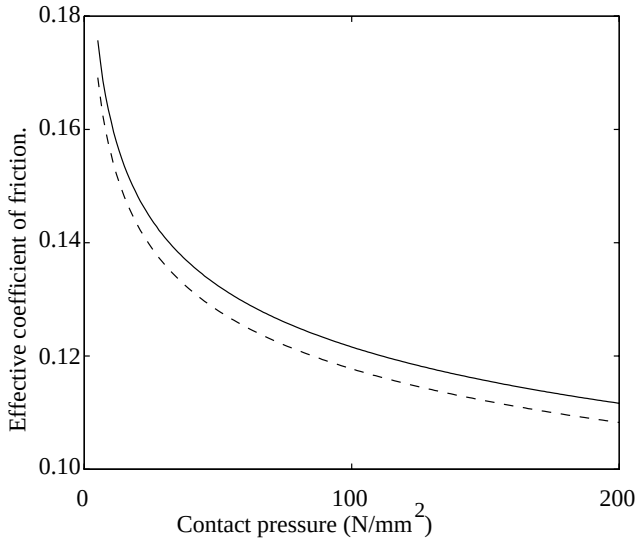

Figure 9: Equivalent Amontons' coefficients of friction ($\mu = \tau/\sigma$) for Kevlar 49-on-aluminium.

However if an equation of the form given in eqn. (11) is fitted only to the points most relevant to a Parafil termination, which here is taken to be all those greater than 6N/mm^2 (21 static and 21 dynamic), then the following refined equations are obtained (where τ and σ are in kN/mm^2):

$$\tau_s = 0.099\sigma^{0.91} \tag{16}$$

$$\tau_d = 0.095\sigma^{0.91} \tag{17}$$

These equations are plotted in Fig. 8, the solid line being the static friction and the dashed line the dynamic. Because the static and dynamic indices are the same, these equations give a static friction greater than the dynamic one for all contact stresses. Note, the axes show mean contact and frictional stresses as a means of visualising the experimental data; the stresses continuously vary along the length of the contact zone, a fact which is included in this analysis.

3.4..1 Expressing μ in terms of a and β.

Equations (16) and (17) can be re-expressed to give equivalent coefficients of friction, μ, as follows:

$$\text{static} \quad \mu_s = a_s\sigma^{\beta_s - 1} = 0.099\sigma^{-0.09} \tag{18}$$

$$\text{dynamic} \quad \mu_d = a_d\sigma^{\beta_d - 1} = 0.095\sigma^{-0.09} \tag{19}$$

These curves are plotted in Fig. 9 for the range of stress encountered in the finite element analysis.

4. Yarn-on-yarn friction for Kevlar 49.

There is no published data in the literature for the yarn-on-yarn friction for Kevlar 49, nor for the shear yield stress. However, because there is minimal yarn-on-yarn slip within a Parafil termination, this parameter is not critical. This is unlike the yarn-on-solid friction, which is a major factor in the functioning of the terminations.

For use in the finite element analysis, a coefficient of friction of μ=0.3 was assumed for the Kevlar-on-Kevlar friction. The rope is modelled as three separate layers, to allow for any relative slip, it is seen in that the shear stress in these layers remains below 25N/mm^2, a value which is believed to be used in the design of Parafil terminations [1]. No slip between these rope layers is indicated in the analysis, so this value is a reasonable assumption. If a lower value of μ was to be used, then slipping would occur before the shear stress could rise to this limiting value; if a higher value was set, then the analysis would be unaffected.

5. Abrasion of polymeric fibres.

Abrasive wear is said to happen when there is a progressive loss of material from the softer surface when two surfaces are rubbed back and forth. In a 'clean' environment this is most often caused by the hard protuberances of one surface gouging grooves in the softer surface as they are reciprocated under normal loading. The swarf is initially pushed to one side but after many cycles it is removed altogether. If grit is present then this process is speeded up, but Parafil terminations are usually sealed to prevent water penetration, so no grit will be able to get in. Subsurface wear can also accrue from fatigue crack growth in the deformed contact region. In polymers, strong adhesion occurs at the points of contact of the asperities; when sliding occurs, fragments are torn from the softer surface and

are left deposited on the harder one [14]. These two classes of wear mechanism, involving subsurface and surface deformation respectively, are termed cohesive and interfacial wear.

6. Archard wear equation

Either by looking at the contact between asperities, or by looking at the wear caused by many abrasive particles it is possible to form the Archard wear equation:

$$Q = \frac{KW}{H} \tag{20}$$

This relates the volume worn per unit sliding distance, Q, to the normal load, W, and the hardness of the softer surface, H. K is the dimensionless wear coefficient. However the dimensional wear coefficient $k = K/H$ is often more useful in engineering because of the difficulty in defining the plastic hardness H of elastomeric materials. k has the units $\mathrm{mm}^3(\mathrm{Nm})^{-1}$ and represents the volume of material removed by wear per unit distance slid per unit normal load.

The shear yield strength of Kevlar 49 is $160\mathrm{N/mm}^2$ [16]. Taking the uniaxial yield stress of the aluminium alloy used for the termination to be $600\mathrm{N/mm}^2$, then its shear yield strength is $300\mathrm{N/mm}^2$ [17]. Therefore the Kevlar fibres are the softer material and will suffer most of the abrasion.

Thermal failure can be avoided (and hence lifetimes improved dramatically) if adequate cooling is provided either by a fan or by water. For Kevlar 29, Du Pont [18, 19] have recorded only small reductions in the tensile strength up to 180°C of about 20% followed by large reductions above this; Kevlar 49 is similar.

Even at the very high stresses, 5-70%, and frequencies, 0.33Hz, to which Crawford and McTernan [11] subjected a 150 tonne Parafil F (Kevlar 29) rope, the temperature did not rise above 100°C due to Kevlar's low hysteresis and the absence of lay geometry. Thermocouples were inserted into the rope core at the front face of the termination. Thermal failure would not be expected to occur at this temperature, and the ropes failed by mechanical abrasion. They reported only split fibres, which would be expected in a fretting failure at low amplitudes of motion.

7. Kevlar 49 on aluminium abrasion

A comprehensive study of abrasion of Kevlar 49 yarn on aluminium has been undertaken. There are many variables that may affect the lifetime of a yarn rubbing on a solid; the amplitude of the cycle, the contact pressure, the maximum load and hence the amount of yarn to be abraded, the surface finishes of the materials including the 'size' that is applied to the yarn, the temperature, the presence of debris and the presence of water. For this analysis it was assumed that only the amplitude, the contact pressure and the thickness to be abraded, are significant variables.

Actual rope yarns were used, with no alteration made to their surface coatings; the materials were kept as clean and dry as possible, and all tests were performed at room temperature (although the temperature in a rope under cyclic loading may rise to 100°C).

For this analysis it is assumed that the rate of wear is uniform throughout a test. This is a reasonable assumption to make as the Kevlar debris is removed from the aluminium surface by the rubbing of both the yarns in these tests and the yarns in the rope terminations, thus ensuring fresh material is always in contact. Also, the Kevlar away from the contact zone moves as one and does not abrade against itself, so whilst it is away from the aluminium surface it is unaffected by the number of cycles accrued.

7.1. Apparatus

Figure 10 shows a schematic view of one station on the abrasion tester that was built to perform lifetime tests on 8 stations simultaneously. Unfortunately, it was soon found that when the first station failed the others would rapidly follow due to the shock loading from a 20kg mass being released from the system. All the abrasion tests were therefore performed on one station running alone.

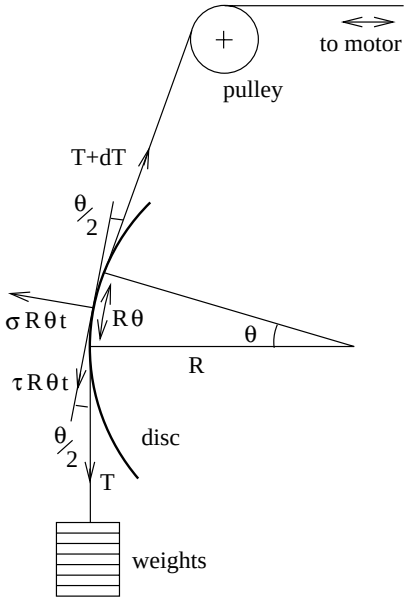

Figure 10: Schematic of apparatus used to determine yarn-on-solid abrasion.

A yarn was passed over a disc of the desired radius, to make the desired contact angle. For small angles of contact the exact value is not relevant in determining the contact pressure, however the contact zone should

be long enough such that a portion of yarn is subjected to the entire regime. If a piece of yarn passed outside the contact zone at both ends of the cycle then no part of the yarn would be fully abraded. The contact length must also be short enough that the tension in the yarn does not rise too much, due to friction, to affect the contact pressure. A contact angle of 10^o was used throughout.

Considering a small element of yarn passing over the disc and resolving normal to the surface, $\sigma R\theta t = 2.T.\theta/2$, or $\sigma = R/Tt$. R is the radius of curvature, T is the yarn tension, σ is the contact stress, and t is the width of the contact zone, which was taken to be 1mm here.

The yarn was guided over the disc by means of pulleys such that it was free to move along its axis only. One end was driven by a motor via an eccentric axle, which gave rise to a sinusoidal oscillation. The movement was constrained with bearings to translate this rotation into a linear motion. The other end was loaded by a free weight. To stop the free weight spinning and hence removing all the twist present in the yarn, it was loosely tied to a cut-off switch with a piece of thick wire. The weight would rotate round by a quarter of a turn until the wire exerted enough torque to prevent the yarn untwisting further; the wire was set such that it provided no axial load into the system. When the yarn eventually broke, this piece of wire would pull a block out of a cut-off switch thus stopping both the motor and the counter. The counter was driven by a reed switch and a magnet attached to the shaft of the motor.

A marker was attached to the yarn just above the weight, and the upper and lower limits of this marker noted by lining up the cross hairs of a travelling microscope; the position was read from the vernier scale on the side of the microscope. These readings were repeated six times and a mean taken to give the amplitude of each cycle.

All the abrasion tests were performed using Kevlar 49 yarn from a bobbin used to make Parafil ropes provided by Linear Composites Ltd. Therefore the number of fibres present, the amount of twist and the size applied to the yarns are all representative of those within a Parafil termination. When assembling the apparatus care was taken to ensure that the number of twists in the yarn remained constant (there are about 45 twists per metre.) The aluminium discs were prepared by sawing a template out of Dural, then turning this in a lathe.

The actual surface of an aluminium 60 tonne Parafil G spike has small shallow grooves running around it every 0.25mm. It was not practical to machine these on the discs used here, as they are a by-product of the turning process in manufacturing the spike. Experiments were done with score marks running perpendicular to the direction of slip, but it was not possible to create the smooth score marks that are found on the spike, and so the lifetimes were exceedingly short.

The discs here were smoothed as much as possible for the first test, and after several abrasion tests were performed it could be seen that the already smooth surface was polished even more by the abrasion from the Kevlar. A fine yellow dust was present around the contact zone from the debris.

The yarn is clamped at both ends between aluminium plates that are screwed together; this is a very efficient method of restraining the ends, as this restraint remains effective regardless of the number of fibres that have broken. It was found to be impractical to glue the ends as it was very difficult to achieve a uniform coating on all the fibres whilst maintaining their geometry within the yarn. A speed of 120rpm was chosen, this being the highest speed possible before dynamic effects from the flexibility of the rig became significant. The change in tension due to the dynamic loading on the free weight is negligible at this speed.

For the fixed amplitude experiments the peak to peak amplitude was fixed at 0.68mm and the contact pressure and thickness to be abraded were altered by using discs of radii 27.5mm and 79.5mm, with loads of 50.0, 100.2, 150.0 and 199.8N. Other experiments were done using peak to peak amplitudes of 0.12, 0.68 and 2.90mm. These having very small maximum sliding speeds of 0.75, 4.27 and 18.2mm/s ($= 2\pi f(a_0/2)$).

7.2. Calculation of wear rate

For this analysis it is assumed that under a certain severity, determined by the contact pressure and the amplitude, the rate of wear of the Kevlar 49 is constant. This is not necessarily true; the rate may slow down due to a build-up of debris which will act as a lubricant and as a barrier, and conversely the rate may speed up due to damage being accumulated above the contact zone from inter-fibre fretting.

The cross sectional area of the yarn is taken to be 0.23mm^2. This area correlates with the breaking load of 440N (taken from a mean of 6 tensile tests using Amaniampong's jaws [20]) and the rope's ultimate tensile stress of 1926N/mm^2. It is assumed that the yarn deforms over the capstan into a rectangle 1mm wide and 0.23mm thick, which is consistent with observations for all the severities measured.

For the yarn experiments, the thickness that needs to be abraded before failure occurs is related to the maximum tension in the yarn. For a larger tension less material needs to be abraded before the remaining yarn reaches its breaking stress. The proportion of yarn that has abraded at failure is (1-$\lambda_{max}/100$) where λ_{max} is the percentage ratio of the maximum load to the breaking load, therefore the thickness that has been abraded, δ, is $\delta/0.23 \times (1 - \lambda_{max}/100)$.

The wear rate is calculated from this thickness as

follows:

$$\text{volume abraded} = r\theta\delta t \tag{21}$$

$$\text{normal load} = T\theta \tag{22}$$

$$\text{distance slid} = 2a_0N \tag{23}$$

where r is the radius of the capstan, θ is the angle of contact zone subtended, t is the width of the contact zone, T is the tension in the yarn, a_0 is the peak to peak amplitude of cycling and N is the number of cycles to failure. Therefore:

$$\begin{aligned} k &= \frac{\text{volume abraded/distance slid}}{\text{normal load}} \\ &= \frac{r\delta t}{2a_0NT} \end{aligned} \tag{24}$$

7.3. Lifetimes of terminations

Very little data has been published for the abrasion lifetimes of Parafil ropes. Some data has been obtained for tests performed at the National Engineering Laboratory on Parafil G ropes. These include tests on 6 tonne ropes with cyclic ranges of 5-35%, 10-50%, 25-55%, 20-60%, 10-70% [21], 15-45%, 5-55% [22], and 15-65% [23]; and 60 tonne ropes cycled between 5-30%, 5-35%, 5-40%, 5-50%, 5-70% [24]. (An x% load, refers to x% of the nominal breaking load of the rope.)

There is no overall scheme to this data, since different maximum and minimum load limits were used throughout. The data for these 6 and 60 tonne Parafil G ropes is plotted in Fig. 11; the y-axis is taken to be the maximum load. (The ranges do not form smooth zones because the minima are different.) It is clear that the 60 tonne ropes have a much shorter lifetime than the 6 tonne ropes. This is due to the larger amplitude of abrasion that is occurring within them.

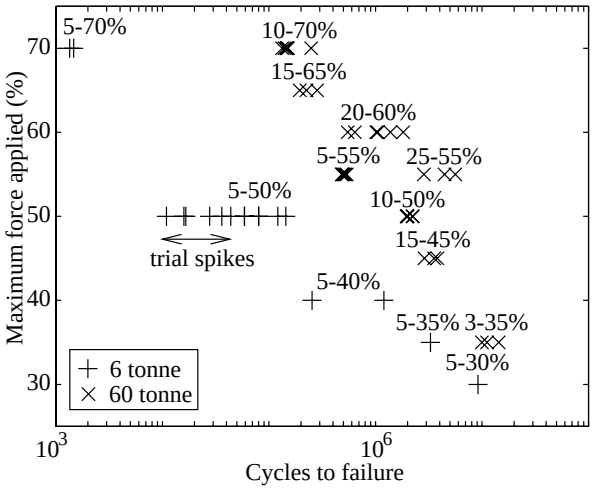

Figure 11: The lifetimes of 6 and 60 tonne Parafil G ropes subjected to cyclic loading.

For the 6 tonne rope, the greatest lifetimes are achieved by the regimes having a 30% cycle (λ=5 to 35, 15 to 45 then 25 to 55 (where λ is the percentage ratio of load to maximum static strength)); next come the regimes with 40% cycles (λ=10 to 50 then 20 to 60) followed by 50% (λ=5 to 55 and 15 to 65) then finally the 10 to 70% cycle. This indicates that it is the amplitude of the cycle, both in terms of load and therefore slip, that is more significant than the maximum load. All the 25 to 55% tests outlived all the 10 to 50% tests, due to their smaller amplitude, despite having a greater maximum load. They also outlived the 5 to 55% tests by an order of magnitude.

7.4. Calculation of wear rate

Using the results from a finite element analysis [1], it is possible to predict a maximum yarn-on-spike amplitude of movement and associated contact pressure for each of these rope tests. The contact pressure is determined maximum preload that has been applied. It is not known what each maximum preload was for the literature data, so for this analysis it is assumed that the maximum load in the cycle is also the limit of the preload. It is assumed that the contact stresses in the termination are solely determined by the maximum load applied, and are not size dependent; i.e. a 6 tonne rope at 50% load will have the same contact pressure between the rope and spike as a 60 tonne rope at 50% load. The contact pressure – preload relationship can be linearised to give:

$$\sigma = 1.30 \times \lambda_{max} \tag{25}$$

where λ_{max} is the maximum percentage load factor applied (100×maximum load/breaking load), and σ is the contact pressure between the spike and rope, and between the rope and barrel in N/mm^2.

To estimate the amplitude of slip it is found from the finite element analysis that there is a position on the spike where no relative slip occurs. If it is assumed that this is the case for 6 tonne ropes as well, and for all the regimes, then the slip can be quickly estimated by analysing the portion of rope between this location and the nose of the spike. Figure 12 shows a schematic diagram of the forces that are present in the fibres at the load cycle limits for a 60 tonne Parafil G rope. From the finite element analysis it is noted that the rope remains static at 163mm and rubs over the nose at 220mm, so 57mm of rope is stretched.

At the salient non-moving location, the axial stress in the rope is assumed to remain constant. At the nose of the spike the load in the rope varies between λ_{max} and λ_{min}. The friction is taken to be uniform along the length of the slipping region. Therefore, the tension in the fibres will vary linearly along their length. Hence the load at the non-moving point will be the mean of λ_{max} and λ_{min}, as seen in Fig. 12 (assuming an equal friction applies in both directions).

The extension in the fibres can be calculated by integrating the strain along the stretched portion. Due

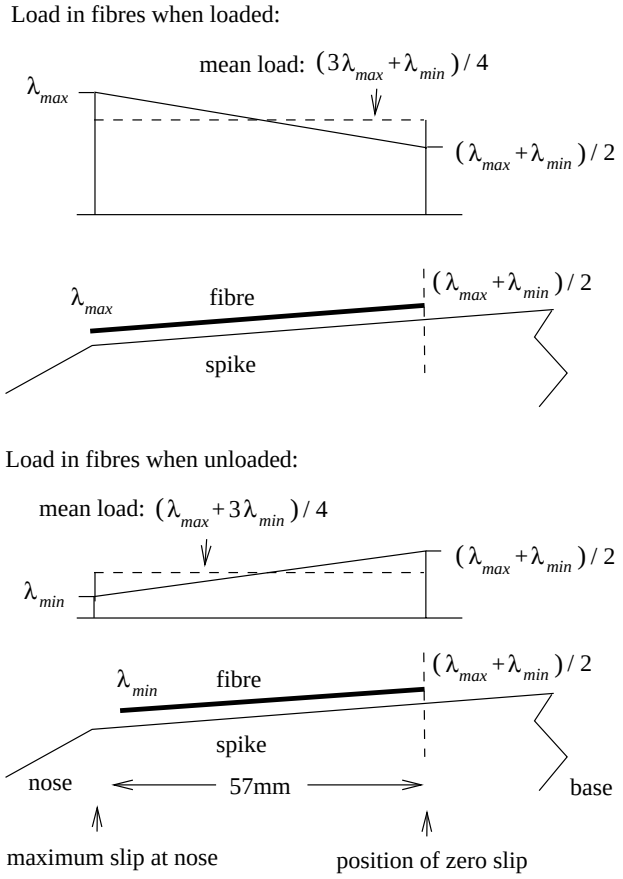

Figure 12: Schematic of the idealised load variation within a termination.

to the assumed linearity, the mean load in the rope can be used to calculate the extension. The maximum load case is equivalent to a uniform load of $(3\lambda_{max} + \lambda_{min})/4$, and the minimum to $(\lambda_{max} + 3\lambda_{min})/4$. The difference between these gives the magnitude, λ_0, for an equivalent uniform cyclic loading of $(\lambda_{max} - \lambda_{min})/2$.

The longitudinal failure strain, ϵ_y, of Kevlar 49 is 0.015, therefore the total cyclic strain ϵ_0, is:

$$\epsilon_0 = \frac{\lambda_0}{100}\epsilon_y = \frac{\lambda_{max} - \lambda_{min}}{2 \times 100}\epsilon_y \qquad (26)$$

Multiplying ϵ_o by the length of the stretched region, 57mm, gives the amplitude of slip, a_o;

$$a_o = 57\epsilon_0 = 4.28 \times 10^{-3}(\lambda_{max} - \lambda_{min}) \qquad (27)$$

For a 5-50% cycle in a 60 tonne rope this gives a displacement of 0.19mm compared with the finite element result of 0.20mm.

It is assumed that the areas of different sized terminations are scaled linearly, such that the cross sectional area of a rope of size, Q tonnes, will be related to a 60 tonne rope by the factor $Q/60$. Therefore the lengths will be scaled by a factor of $\sqrt{Q/60}$.

Hence the amplitude of slip becomes:

$$a_o = 57\epsilon_0 = 4.28 \times 10^{-3}(\lambda_{max} - \lambda_{min})\sqrt{Q/60} \qquad (28)$$

The compressed thickness of the rope at the nose of a 60 tonne Parafil G rope is 3.2mm from the finite element analysis (which is an annulus of 320mm^2 at a mean radius of 16mm). The thickness to be abraded, δ, that needs to fail from each side of the rope, for the yield stress to be reached in the remaining rope at the maximum load, is given (for a rope of size Q tonnes) by:

$$\delta = 3.2 \times \frac{100 - \lambda_{max}}{100} \times \frac{1}{2} \times \sqrt{\frac{Q}{60}} \qquad (29)$$

It is assumed that an equal amount of wear takes place between the rope and spike and the rope and barrel. Therefore the wear rate is calculated by looking at the contact between the rope and the spike only. The wear rate is calculated from this thickness as follows:

$$\text{volume abraded} = l2\pi r\delta \qquad (30)$$

$$\text{normal load} = 2\pi r l\sigma \qquad (31)$$

$$\text{distance slid} = 2a_0N \qquad (32)$$

where r is the radius of the spike ($= 16.0 \times \sqrt{Q/60}$), l is the length of contact zone, a_0 is the peak to peak amplitude of cycling and N is the number of cycles to failure. Therefore:

$$k = \frac{\text{volume abraded/distance slid}}{\text{normal load}} = \frac{\delta}{2\sigma a_0 N} \qquad (33)$$

8. Ratner-Lancaster correlation

The product of the ultimate tensile stress and elongation for the polymer, σ_u and ϵ_u, is roughly proportional to the area under the stress-strain curve to the point of tensile rupture, and so provides a measure of the work done in producing tensile rupture. Despite the conditions of measurement of these quantities varying from the conditions under which abrasion takes place it is found for many polymers that there is a good agreement between $1/\sigma_u\epsilon_u$ and k, [25].

The transverse properties of Kevlar 49 are σ_u=2500N/mm^2 and ϵ_u=0.021 [26]. This leads to an estimated k of 1.0×10^{-3}mm^3(Nm)$^{-1}$ [25].

9. Wear rate versus load

Figure 13 shows the average wear rate for each test against the normal load. There are three distinct groups present, these are due to the vastly different normal loads present in the capstan, 6 tonne and 60 tonne rope experiments. The three groups lie on a line whose gradient is similar to those found for

PTFE and Nylon 6 sliding against a mild steel counterface [27], these being represented by the dashed lines.

From this it can be seen that the wear rate increases with normal reaction. Archard's equation implies that the wear rate should be directly proportional to the normal load, i.e. a log-log graph should have a gradient of unity. The gradient here is slightly less than this, although it is considered close enough for the use of Archard's equation.

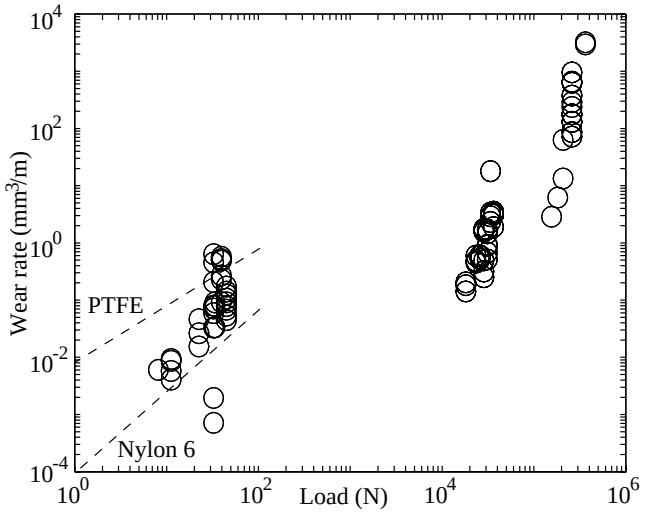

Figure 13: Effect of normal load on wear rate.

10. Dimensional wear coefficient versus amplitude

For metals the wear rates depend on the amplitude of the sliding. At amplitudes less than 1μm the two surfaces are stuck and negligible wear takes place. Up to 10μm, microslip starts occuring with a rise in wear rate. Between 10μm and 300μm, gross slip occurs and there is a large rise in k. Beyond this level reciprocating sliding is occuring and the value of k has generally plateaued. For reference with Kevlar, steel on steel wear is shown on Fig. 14, [28].

The relationship between the dimensional wear coefficient, k, of Kevlar 49 on aluminium and the peak to peak amplitude of reciprocal motion is shown in Fig. 14. There is no plateau evident — there is a uniform rise in the dimensional wear coefficient with amplitude, the values being typically one to two orders of magnitude greater than steel-on-steel for the range of displacements measured.

The Ratner-Lancaster prediction of $1.0 \times 10^{-3}\text{mm}^3(\text{Nm})^{-1}$ lies in the middle of the values of k observed.

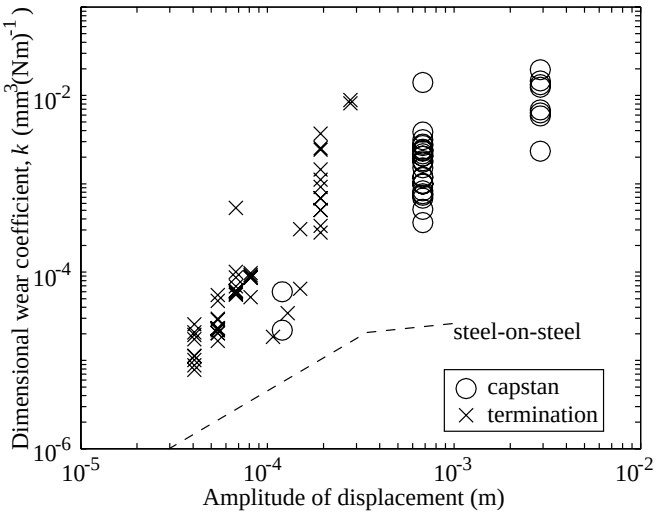

Figure 14: Effect of ampitude on dimensional wear coefficient.

11. Creep rupture effects

At high stresses, creep-rupture may be a significant factor. Kenney et al. [29] have carried out a multitude of tests on nylon fibres, yarns and small ropes, subjecting them to a cyclic axial stress. They found that their yarns and single fibres fail by a creep-rupture mode (i.e. they creep to failure) which depends on the total time that the loads are applied rather than the number of cycles. They also showed that the behaviour of other oriented fibres including polyester and aramid (e.g. Kevlar) agrees with this cumulative time under load model.

Lyons et al. (reported in [30]) have shown that there are two distinct regions in the strain – cycles-to-failure curve, with extremely long lives occurring for low strains. Kenney et al. cycled across these two regions, thus masking this phenomenon.

Crawford and McTernan [11] performed low-load cyclic tests at different frequencies, thus subjecting the ropes to different times under load. They found no discernible difference in the lifetimes. Cyclic loading at high stresses is not on the agenda for the current uses of Parafil so creep-rupture has not been a part of this study.

12. Conclusions

1. With the appropriate experiments it is possible to gather the friction data that is required for a finite element analysis of a Parafil termination. For Kevlar 49-on-aluminium this takes the form $\tau_s = 0.099\sigma^{0.91}$ and $\tau_d = 0.095\sigma^{0.91}$. Kevlar 49-on-Kevlar 49 friction is not so critical in the mechanics of the terminations as it is greater ($\mu \rightarrow 0.22$ at high pressures).

2. In a similar way, Kevlar 49-on-Kevlar 49 abrasion is not assumed to be the critical factor in the lifetimes of terminations, Kevlar 49-on-aluminium abrasion is. The wear rate is directly proportional to the normal load therefore Kevlar 49-on-aluminium abrasion can be expressed in terms the Archard wear equation.

3. The dimensional wear coefficient depends stongly on the amplitude of slip present rising from $1.0 \times 10^{-5}\text{mm}^3(\text{Nm})^{-1}$ at 40μm to $1.0 \times 10^{-2}\text{mm}^3(\text{Nm})^{-1}$ at 3mm peak to peak displacement.

4. This work, which focussed on understanding behaviour, can therefore be extended to optimise the design of Parafil terminations in terms of materials and geometry for bigger and longer lasting ropes.

References

[1] I.F. Brown, Abrasion and Friction in Parallel-lay Rope Terminations, PhD Thesis, CUED, 1997.

[2] I.M. Hutchings, Tribology, Friction and Wear of Engineering Materials, Edward Arnold, London, 1992.

[3] B.J. Briscoe and F. Motamedi, The ballistic impact charateristics of aramid fibres: the influence of interface friction. Wear, 158, 1992.

[4] F. Van De Velde and P. De Baets, The friction and wear behaviour of polyamide 6 sliding against stell at low velocity under very high contact pressures, Wear, 209, 1997.

[5] I.V. Kragelsky, M.N. Dobychin and V.S. Kombalov, *Friction and wear, calculation methods.* Pergamon Press, Oxford. 1982.

[6] B. Lincoln, Frictional and elastic properties of high polymeric materials. British Journal of Applied Physics, Vol. 3 Aug. 1952.

[7] H.G. Howell, and J. Mazur "Amonton's law and fibre friction." Journal of the Textile Institute, Vol. 44 No. 2, 1953.

[8] H.G. Howell, The general case of friction of a string round a cylinder, Journal of the Textile Insitute, Vol 44 No8/9, 1953

[9] B. Piller, *Bulked yarns.* Textile trade press, Manchester. 1973.

[10] D.E. Beers and J.E. Ramirez, "Vectran fiber for ropes and cables." Marine Technology Society '90 Proceedings, Washington. 1990.

[11] H. Crawford and C.M. McTernan, "'Fatigue' properties of Parafil." Symposium on engineering applications of Parafil ropes, London. 1988.

[12] M.J. Schick, "Surface characteristics of fibres and textiles. Part I." Marcel Dekker, Inc. New York. 1975.

[13] M.J. Schick, "Surface characteristics of fibres and textiles. Part II." Marcel Dekker, Inc. New York. 1977.

[14] R. Meredith and J.W.S. Hearle, "Physical methods of investigating textiles." Textile Book Publishers, New York. 1959.

[15] D.G. Lyne, "The dynamic friction between cellulose acetate yarn and a cylindrical metal surface." Journal of the Textile Institute, Vol. 46 No. 1, 1955.

[16] S. Kawabata and M. Sera, "Torsional Fatigue of Aramid Fibers." Proceedings International Conference on Advanced Composites, Wollongong University, Australia. 1993.

[17] M.F. Ashby and D.R.H. Jones, "Engineering Materials 1." Pergamon Press. 1980.

[18] Du Pont, "Characteristics and uses of Kevlar 29 aramid." E.I. Du Pont de Nemours and Co. Inc., Wilmington, Bulletin No. 375. 1976.

[19] Du Pont, "Kevlar para-aramid; database for fibre optic and other cables." E.I. Du Pont de Nemours and Co. Inc., Wilmington. 1988.

[20] G. Amaniampong, "Variability and Viscoelasticity of Parallel-lay Ropes." PhD Thesis, CUED. 1992.

[21] Technomare, Private correspondence with D. Kingston, Linear Composites Ltd., 1996.

[22] L.M. McTernan, Private correspondence with D. Kingston, Linear Composites Ltd., 1986

[23] L.M. McTernan, "Comparative Tests on 6 tonne Type G Parafil Cables and Terminations." National Engineering Laboratory — private correspondence with D. Kingston, Linear Composites Ltd., 1992.

[24] L.M. McTernan, "Second Interim Report on Testing of 60 tonne Parafil Type G (Kevlar 49) Rope and Terminations." National Engineering Laboratory, 1986

[25] B.J. Briscoe, Wear of polymers: an essay on fundamental aspects, Tribology International 14, 231-243 1981.

[26] S. Kawabata, M. Sera, T. Kotani, K. Katsuma, M. Niwa and C. Xiaoxin, Anisotropic Mechanical Properties of Advanced High Performance Fibers Obtained by a Single Fiber Testing System. 9^{th} International Conf. Composite Materials, Spain 1993.

[27] from D.C. Evans and J.K. Lancaster, in D. Scott (Ed.), Wear, Treatise on Materials Science and Technology, Academic Press, 13, 85-139, 1979.

[28] O. Vingsbo and S. Söderberg, in K.C. Ludema, Wear of Materials 1987, ASME, pp. 885-894, 1987.

[29] M.C. Kenney, J.F. Mandell and F.J. McGarry, "Fatigue behaviour of synthetic fibres, yarns, and ropes." Journal of Material Science, 20, pp. 2045-2059, 1985.

[30] J.W.S. Hearle, "Fatigue in fibres and plastics (a review)." Journal of Material Science, 2, pp. 474-488, 1967.